metals

MDPI

Article

Effect of Solution Treatment on Microstructure Evolution of a Powder Metallurgy Nickel Based Superalloy with Incomplete Dynamic Recrystallization Microstructure

Yanhui Liu [1,2,*], Miao Wang [1], Pengwei Sun [1], Guang Yang [1], Wenjie Song [1] and Xiaofeng Wang [1]

[1] College of Mechanical & Electrical Engineering, Shaanxi University of Science & Technology, Xi'an 710021, China
[2] School of Materials Science and Engineering, Northwestern Polytechnical University, Xi'an 710072, China
* Correspondence: liuyanhui@sust.edu.cn; Tel.: +86-29-86168976

Abstract: In this paper, the powder metallurgy (P/M) Ni-based superalloy FGH4096 with an incomplete dynamic recrystallization structure was treated by a solution treatment at different temperatures, cooling methods, and holding times. The size, morphology, and distribution of grains and γ′ precipitates were characterized by an optical microscope (OM) and a scanning electron microscope (SEM). Research results showed that with the increase of solution temperature from 1060 °C to 1100 °C, the degree of recrystallization increased continuously, the distribution of grain became uniform, and a large number of annealing twins were found. At the same time, the degree of redissolution of the primary γ′ precipitates at the grain boundary increased, and the size of secondary γ′ phase reprecipitated within the grain decreased. The morphology of the secondary γ′ precipitates is mainly spherical with a single distribution under air cooling (AC), while the morphology is near-spherical, cuboids, octets, petaloid, and dendrites with a bimodal distribution under furnace cooling (FC). The size of the γ′ precipitates decreased and the volume fraction increased with the extension of holding time at a higher solution temperature (1100 °C).

Keywords: P/M Ni-based superalloy; incomplete dynamic recrystallization; solution treatment; γ′ precipitates

check for updates

Citation: Liu, Y.; Wang, M.; Sun, P.; Yang, G.; Song, W.; Wang, X. Effect of Solution Treatment on Microstructure Evolution of a Powder Metallurgy Nickel Based Superalloy with Incomplete Dynamic Recrystallization Microstructure. *Metals* **2023**, *13*, 239. https://doi.org/10.3390/met13020239

Academic Editor: Angelo Fernando Padilha

Received: 28 November 2022
Revised: 5 January 2023
Accepted: 17 January 2023
Published: 27 January 2023

Copyright: © 2023 by the authors. Licensee MDPI, Basel, Switzerland. This article is an open access article distributed under the terms and conditions of the Creative Commons Attribution (CC BY) license (https://creativecommons.org/licenses/by/4.0/).

1. Introduction

Nickel-based powder metallurgy superalloys solve the problems of severe segregation, uneven structure, and poor hot workability commonly existing in traditional cast superalloys. It has a series of advantages, including no macro segregation, uniform structure, and fine grain. It has become the preferred material for preparing key hot end components, such as high thrust weight ratio and high-performance aero-engine turbine disks [1–4]. In recent years, with the rapid development of aero-engine technology, higher requirements are put forward for the performance indexes of P/M superalloys, and the balanced development of high temperature strength, plasticity, creep, and fatigue crack resistance is increasingly pursued [5]. FGH4096 is a γ′ precipitation strengthening nickel-based powder superalloy, which is representative of the second-generation nickel-based powder superalloys in China. FGH4096 alloy can serve up to 750 °C. It has excellent comprehensive properties such as high temperature resistance, high strength and toughness, and low crack growth rate. It is a damage tolerant powder superalloy widely used in the manufacture of advanced aero-engine high-pressure turbines and high-pressure compressor powder discs [6,7]. The Ni-based FGH4096 superalloy has a face centered cubic (FCC) structure and contains about 40 percent coherent precipitates (γ′ phase) of L12 structure within the solid solution matrix (γ phase) [8]. Due to its superb resistance against dislocation shearing, the γ′ phase plays a significant role in improving the high-temperature performance of Ni-based superalloys [9].

It is well-known that the strengthening effect of alloys is closely related to the grain size and the number, size, distribution, and stability of precipitates, and a reasonable heat treatment system is the key to obtain appropriate grain size and precipitates [10,11]. In previous studies, a large number of researchers have discussed the relationship between heat treatment and microstructure evolution of P/M superalloys [12–14]. Tian et al. [15] studied the effect of aging treatment on the microstructure and properties of a novel spray-formed P/M superalloy FGH100L; they found that the grain size of the sub-solvus and super-solvus solution treatments changed little during the long-term aging treatment. As the aging time increases, γ' precipitates are coarsening and splitting. Compared with the super-solvus solution treatment, the sub-solvus had excellent high-temperature tensile properties after long-term aging treatment. Ding et al. [16] studied the effect of cooling rate on the microstructure and tensile properties of nickel-based P/M superalloy CSU-A1 by using two different quenching methods. The experimental results show that the average grain size of oil-quenched and air-cooled specimens is almost the same. The tensile strength of oil-quenched specimens at room temperature is higher than the equivalent tensile strength of air-cooled specimens, but the difference between them tends to be the same as the temperature rises to 650 °C. Huang et al. [17] studied the effect of cooling rate on the microstructure and tensile properties of an FGH98 nickel-based P/M superalloy at 750 °C. The results showed that with the decrease of cooling rate, the average size of the secondary γ' precipitates increase, and the morphology changes from a near-cuboidal shape to a butterfly shape. Han et al. [18] studied the effect of heat treatment on the microstructure and properties of a P/M Inconel 718 superalloy. Zhang et al. [19] optimized the microstructure and tensile properties of MIM418 P/M superalloys through a heat treatment process. Hao et al. [20] studied the effect of heat treatment on the microstructure and mechanical properties of nickel-based P/M superalloys melted by a selective laser.

The above studies on various P/M nickel-based superalloys have discussed the relationship between the heat treatment process and microstructure evolution from different perspectives, but they mainly focus on the microstructure after complete dynamic recrystallization, which has a uniform initial microstructure; however, there are few reports on the heat treatment process with incomplete dynamic recrystallization. In fact, there are great differences in the environment of the turbine disc from the center to the edge under the working state—the disc center is connected with the shaft, with large bearing capacity but relatively low working temperature; the disc edge is in contact with the fuel gas, and the working temperature is higher although the bearing capacity is smaller. Therefore, it is necessary to prepare dual-performance turbine disks that meet the different performance requirements of different parts, that is, the hub part has a fine-grained structure, which has high yield strength and low cycle fatigue performance at low temperatures. The rim has a coarse-grained structure, which has high endurance, creep strength, and crack propagation resistance at high temperatures. Hence, the transition region of coarse and fine grains will inevitably appear in the junction of the rim and hub, which has an incomplete dynamic recrystallization structure, and its performance will directly affect the service life of the turbine disk [21–24]. It is found that proper solution heat treatment after deformation can effectively improve the microstructure and material properties [10,25,26]. Therefore, how to optimize the microstructure of the transition region has become a major problem restricting the further improvement of material properties. Based on this, this paper mainly studies the heat treatment process of the incomplete dynamic recrystallization structure, and analyzes the evolution mechanism of the structure and precipitates, which has important engineering application value for realizing the process control of dual performance turbine disk and promoting its application.

2. Materials and Methods

In this experiment, hot isostatic pressing (HIP) nickel-based P/M superalloy FGH4096 was used. It is a second-generation damage-tolerant superalloy, which has a reduced volume fraction of the γ' precipitates compared with the first-generation FGH4095. Although

sacrificing a certain strength, its crack propagation resistance is significantly improved, its service life is greatly extended, and its service temperature is also increased from 650 °C to 750 °C [27]. The nominal chemical composition of FGH4096 is shown in Table 1. The metal powder was prepared by the plasma rotating electrode process (PREP), and the size of the spherical metal powder particles was about 50–100 μm. The required metal powder is obtained by the plasma rotating electrode process (PREP), and the particle size of the spherical metal powder is about 50~100 μm. After vacuum degassing, the obtained metal powder particles were sealed inside a container of stainless steel, and then processed with HIP at 1120 °C and 130 MPa for 3 h, followed by furnace cooling to room temperature.

Table 1. Chemical composition of the nickel-based superalloy FGH4096 (wt.%).

C	Al	W	Nb	Mo	Ti
<0.030	2.321	4.063	0.832	3.973	3.721
Cr	Co	Fe	B	Mn	Zr
16.213	13.142	<0.510	<0.015	<0.150	0.036
Si	P	O	H	N	Ni
<0.200	<0.015	<0.005	<0.001	<0.005	Bal.

Hot compression experiments were carried out at 1080 °C and 0.001 s^{-1} on the Gleeble-1500D thermal simulation tester. Several Φ8 mm × 12 mm cylindrical specimens were cut by electrolytic discharge machining (EDM) after hot isostatic pressing. In order to obtain an incomplete dynamic recrystallization structure, 30% compression was selected. After compression, the specimens were cut along the central axis, and specimens with the size of 3 mm × 3 mm × 5 mm were taken from the most central area of the section for solution treatment experiment to ensure that the specimens had the same structure before heat treatment. Previous studies have found that the complete dissolution temperature of the primary γ′ precipitates of the FGH4096 superalloy is between 1120 °C and 1140 °C [28–30], so the solution temperature is determined as 1060 °C, 1080 °C, and 1100 °C; the holding times are 1 h and 10 h; and the cooling methods are AC and FC. After the experiment, sand paper with different particle sizes was used for polishing until there was no scratch on the surface. Then, abrasive paste of W1.5 was added to the polishing machine for 30 min. The microstructures were observed using an OLYMPUS DSX510 optical microscope (OM) and the etching solution was 5 g $CuSO_4$ + 50 mL HCl + 25 mL H_2O_2. The morphology of the γ′ precipitates were observed by the TESCAN MIRA3 XMU field emission scanning electron microscope (FESEM) and the electrolytic polishing solution was 30 mL H_2SO_4 + 30 mL HNO_3 + 10 mL H_3PO_4. Image-pro Plus 6.0 software was used to calculate the size and distribution of grains and precipitates.

3. Results and Discussion

3.1. Initial Microstructure

The initial microstructure of the as-HIPed FGH4096 is shown in Figure 1. It can be seen from Figure 1a that the original microstructure is composed of a large number of equiaxed grains, original powder particles, and lamella-like straight annealing twins, with an average grain size of about 32.3 μm. Figure 1b shows the original morphology of γ′ precipitates. It can be seen that the typical microstructure of FGH4096 is mainly composed of a large irregular shape primary γ′ precipitates pinned at the grain boundary, the form of spherical, butterfly-shaped petaloid secondary γ′ precipitates, and a large number of fine tertiary γ′ precipitates with dispersive distribution within the grain. The γ′ precipitates are uniformly distributed in equiaxed grains, original powder particles, and near lamella-like straight annealing twins.

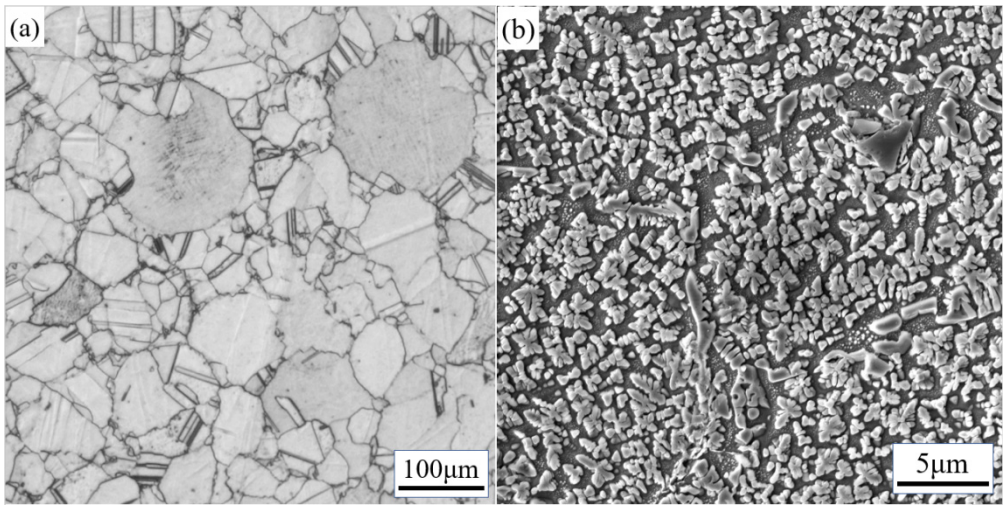


Figure 1. Initial microstructure of the as-HIPed FGH4096: (**a**) grain structure and (**b**) γ' precipitates morphology.

3.2. Effect of Solution Temperature on Microstructure and Precipitates

Figure 2 shows the grain structure before and after solution treatment at different temperatures. It can be seen that the structure before heat treatment is a mixed structure of deformed grains and a large number of dynamic recrystallized grains with very small size. The recrystallized grains are distributed around the deformed grains in a necklace shape. Twins exist in some deformed grains, and the average grain size is about 32.47 μm. After holding at 1060 °C for 10 h, the number and size of recrystallized grains increase obviously, but there are still a large number of deformed grains, with an average grain size of about 28.92 μm and the volume fraction of recrystallization is about 43.26%. At 1080 °C for 10 h, most of the large deformed grains have been eliminated, and some recrystallized grains begin to grow. The average grain size is about 14.64 μm and the volume fraction of recrystallization is about 72.53%. At 1100 °C for 10 h, the deformed grains have completely disappeared, complete recrystallization has occurred, and a large number of annealing twins have appeared. The grains are evenly distributed, and the average grain size is about 24.66 μm.

Figure 3 shows the morphology of γ' precipitates after solution treatment for 10 h at different temperatures by AC. At 1060 °C, primary γ' precipitates on grain boundary are partially dissolved, but a large amount of undissolved primary γ' precipitates remain. The average size of the primary γ' phase is 1–3 μm with smooth profiles, and part of it became spherical or nearly spherical. The secondary γ' precipitates within the grain are spherical with an average size of 274 nm and a small volume fraction. The transformation from multi-shape and multi-size distribution in the initial microstructure to spherical dispersion distribution with uniform and single size indicates that the secondary and tertiary γ' precipitates distribution in the original forged microstructure can be completely redissolved into the matrix during the sub-solvus solution treatment at 1060 °C, and then precipitated in a uniform spherical state during the cooling process. At 1080 °C, only a few small primary γ' precipitates with an average size of 1.24 μm and shape of nearly spherical or cuboidal are left. A few secondary γ' precipitates and a large number of tertiary γ' precipitates are reprecipitated within the grain, the average size of which are 417 nm and 55 nm, respectively, with a spherical distribution and increased volume fraction. At 1100 °C, the primary γ' precipitates at the grain boundary are almost completely dissolved, and the remaining primary γ' precipitates are spherical or nearly spherical with an average size of 252 nm. The average size of secondary γ' precipitates reprecipitated within the grain is 43 nm, and the volume fraction increased significantly.

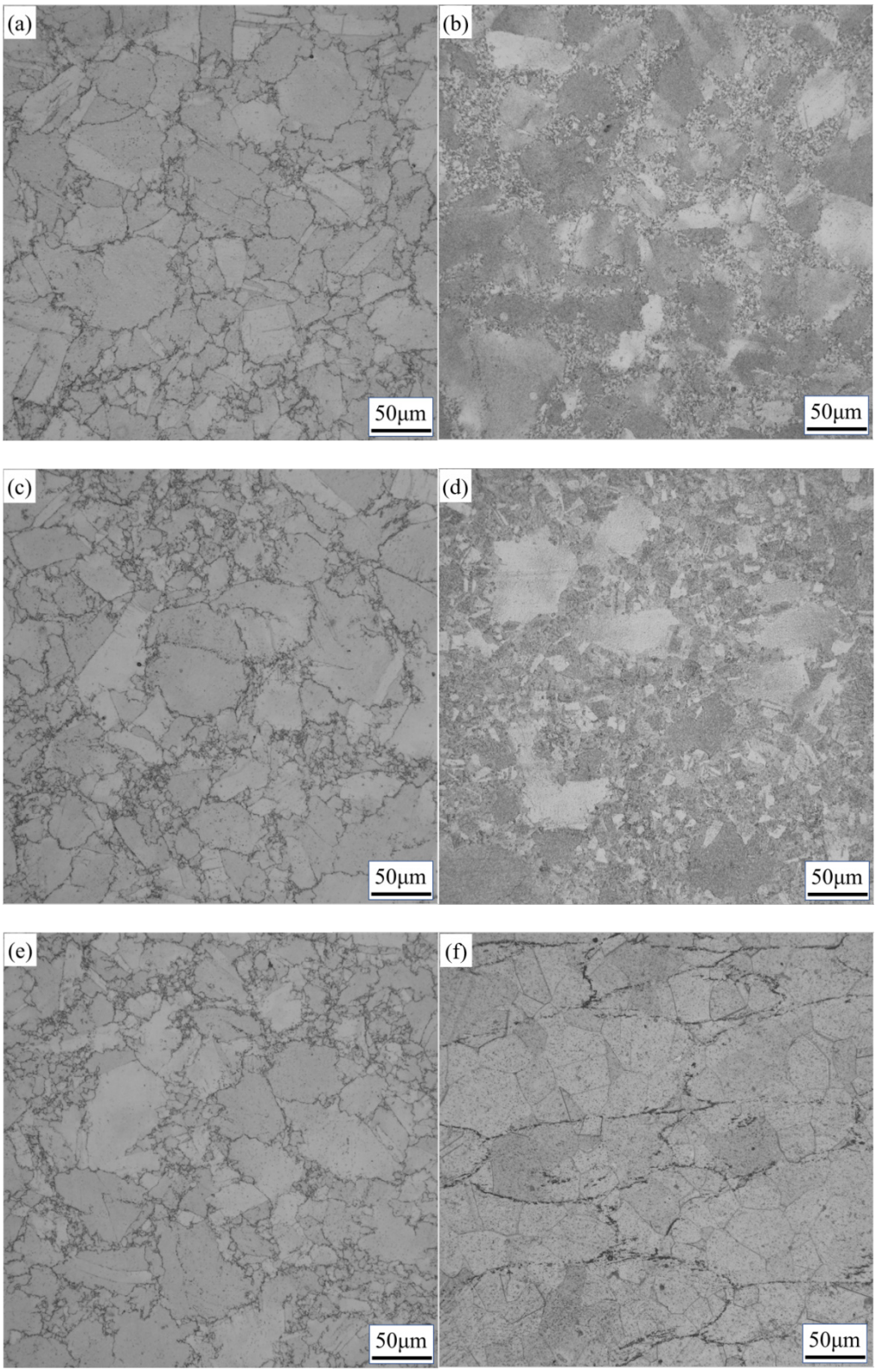


Figure 2. Influence of solution treatment temperature on size distribution of grain: (**a**,**c**,**e**) before solution treatment and (**b**,**d**,**f**) after solution treatment for 10 h; (**b**) 1060 °C, (**d**) 1080 °C, and (**f**) 1100 °C.

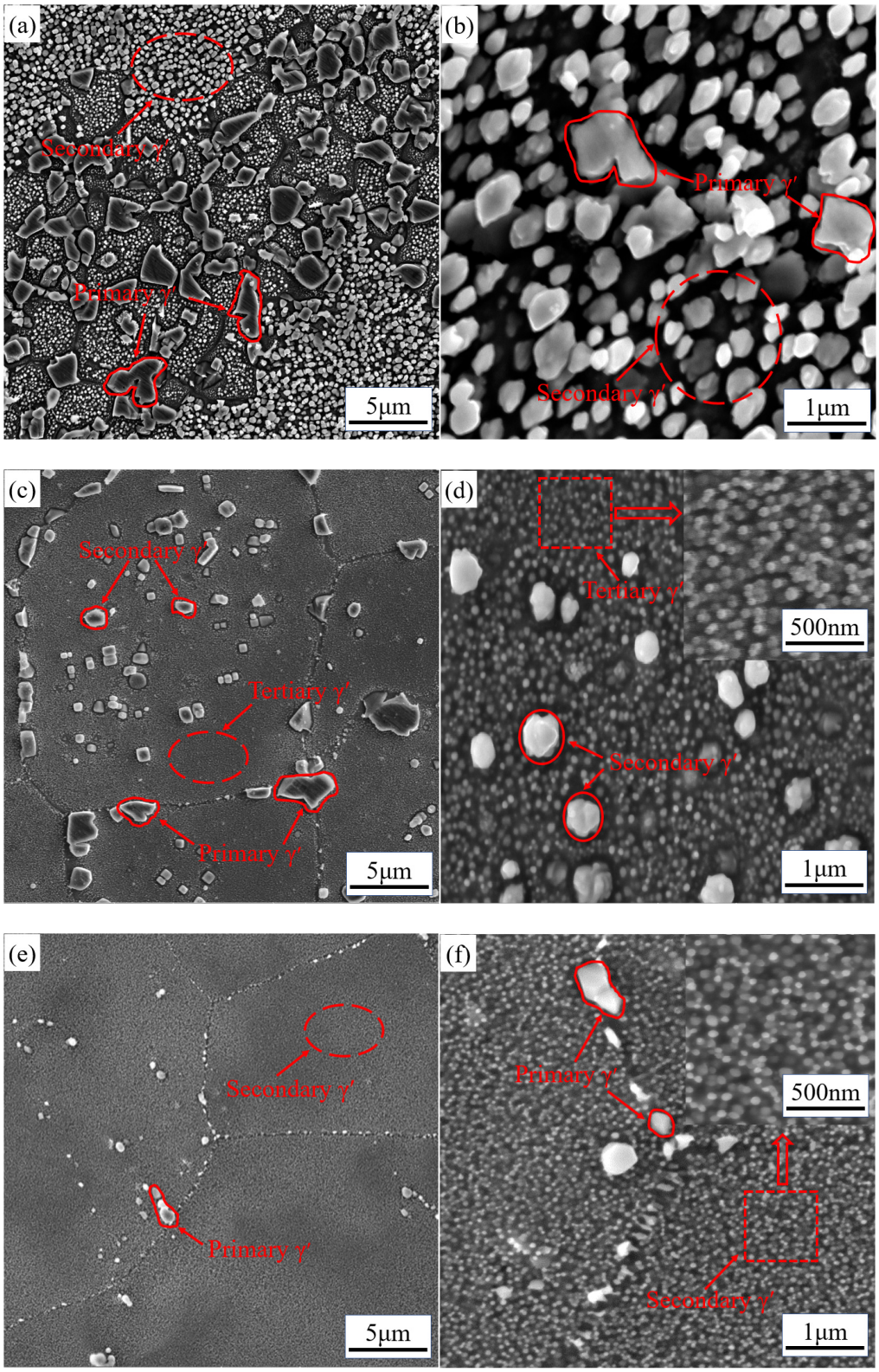


Figure 3. Morphology of γ′ precipitates after solution treatment for 10 h at different temperatures by AC: (**a**,**b**) 1060 °C, (**c**,**d**) 1080 °C, (**e**,**f**) 1100 °C.

The grain size is affected by the degree of recrystallization and solubility of precipitates. At 1060 °C, a large amount of undissolved primary γ′ precipitates on the grain boundary seriously hinder the grain boundary migration process, resulting in a larger grain size and

smaller degree of recrystallization. With the increase of temperature (1080 °C), a large amount of γ′ precipitates are dissolved on the grain boundary, the migration rate of the grain boundary is accelerated, and the serrated grain boundary becomes straight. The increase of recrystallization degree leads to the decrease of average grain size, thus forming a relatively uniform microstructure. The secondary γ′ precipitates within the grain grows, but the volume fraction decreases obviously, with the reprecipitation of a large number of fine tertiary γ′ precipitates. With the further increase of temperature (1100 °C), all of the primary γ′ precipitates on the grain boundary are almost redissolved, and the resistance to grain boundary migration was greatly reduced, with the increase of grain size and smooth grain boundary. The increase of temperature leads to complete recrystallization of grain structure, and a large number of annealing twins are produced, thus forming a uniform but relatively rough microstructure [31]. In addition, a large amount of redissolution of γ′ precipitates cause the supersaturation of the matrix and the nucleation density to increase obviously. The secondary γ′ precipitates reprecipitated under AC have no time to grow, resulting in their relatively small size [17,32].

3.3. Influence of Cooling Mode on Precipitates

Figure 4 shows the morphology of the γ′ precipitates at 1080 °C for 10 h by FC. It can be seen that large γ′ precipitates are partially dissolved on the grain boundary, and the profiles gradually become smooth, with an average size of 1.71 μm. The reprecipitated secondary γ′ precipitates and the fine tertiary γ′ precipitates are distributed within the grain. The secondary γ′ precipitates have a bimodal distribution; the large secondary γ′ precipitates are cuboids, octets, or dendrites, with an average size of 578 nm, and the small size of the secondary γ′ precipitates are near-spherical, octets, or petaloid, with an average size of 234 nm. A large number of tertiary γ′ precipitates can be seen around the small secondary γ′ precipitates, with an average size of about 50 nm. Compared with the morphology of the γ′ precipitates after AC at the same solution temperature and holding time (Figure 3c,d), the quantity and size of the undissolved primary γ′ precipitates on the grain boundary increase after FC, and the secondary γ′ precipitates reprecipitated within the grain present a bimodal and heterogeneous distribution. In addition, the size of the tertiary γ′ precipitates are similar to that after AC.

The volume fraction of γ′ precipitates reprecipitated after FC is obviously smaller than that after AC, indicating that the nucleation density of γ′ precipitates is low under the slow cooling condition. This results in a lower total coherent strain energy, which leads to coarsening of the γ′ precipitates [33]. The slow cooling rate (FC) provides supersaturation and a sufficient diffusion rate, resulting in irregular growth and unstable morphology of the γ′ precipitates during cooling. It can be seen from Figure 4 that a large number of unstable cuboids γ′ precipitates are reprecipitated during cooling, which have a high chemical driving force along the <111> crystal direction during the growth process, and its growth rate is greater than the <100> crystal direction with low chemical driving force. Therefore, the cuboid γ′ precipitates become concave in four <100> crystal directions, that is, the edge of γ′ precipitates have obvious indentation. The elastic stress field distributed in the concave region can strongly trap solute atoms dissolved in the γ matrix and interact with the solute atoms enriched in the elastic stress field to promote the partial dissolution of γ′ precipitates. With the increase of the concave curvature radius, the γ phase gradually permeates into the concave of γ′ precipitates along the <100> crystal direction, leading to phase splitting and gradually forming the cuboid or octet γ′ precipitates [34,35]. The linear arrangement of the cuboid γ′ precipitates indicates that there exists strong interaction between γ′ precipitates.

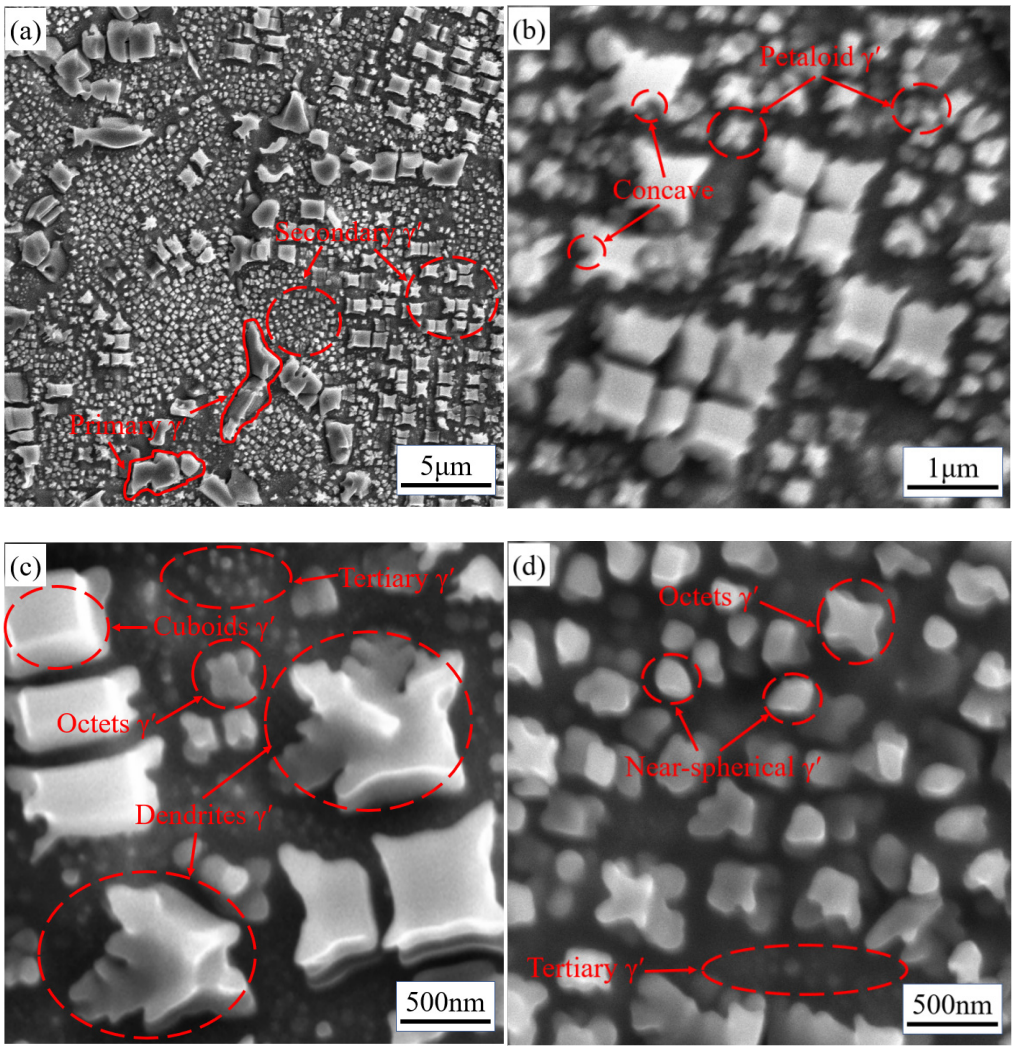


Figure 4. Morphology of γ′ precipitates after holding at 1080 °C for 10 h by FC: (**a**) low magnification, (**b**–**d**) high magnification and feature distribution of secondary γ′ precipitates and tertiary γ′ precipitates.

At the same time, in this slow cooling process, sufficiently high saturation of solid solution elements leads to the rapid diffusion and elastic strain of solute atoms, which together lead to the instability of the γ/γ′ interface, and the split and the unstable growth of γ′ precipitates simultaneously, resulting in the dendritic morphology of the precipitated phase. It can be seen from Figure 4 that the dendrites' growth follows a certain direction, and the growth of these directional dendrites strongly depends on the coherent strain energy induced by lattice mismatch. In the early stage, it was along the <111> direction, resulting in morphological instability, and then formed a concave shape. The concave shape forms a new {100} plane along the <100> direction, releasing the increasing coherent strain energy related to the size of the precipitated phase. The repetition of this process leads to the formation of secondary branches [36,37]. However, due to the relatively high content of γ′ precipitates, the particles inevitably interact with each other, which greatly reduces the probability of γ′ precipitates developing into complete dendrites (Figure 4c) [38], and more of the γ′ precipitates present butterfly dendritic prototypes (Figure 4b). Therefore, the secondary-precipitated γ′ precipitates transform from spherical to near-spherical, cuboids, octets, petaloid, and dendrites with a slow cooling rate (FC). In addition, due to the slow cooling rate, a large number of dense and fine tertiary γ′ precipitates are observed in the matrix channel, and most of the precipitates are spherical with a size of about 50 nm.

3.4. Influence of Holding Time on Precipitates

Figure 5 shows the morphology of γ′ precipitates after holding at 1100 °C for 1 h by AC. The large primary γ′ precipitates on the grain boundary have been dissolved in large quantities, and the remaining primary γ′ precipitates are thin strip or near-spherical with an average size of 526 nm. The average size of the secondary γ′ precipitates precipitated within the grain is 185 nm, and the shape is nearly spherical and cuboidal. Compared with the morphology of γ′ precipitates after holding for 10 h and air cooling at the same temperature (Figure 3e,f), after holding for 1 h, the degree of redissolution of the large primary γ′ precipitates on the grain boundary becomes significantly smaller, and the size of the secondary γ′ precipitates reprecipitated within the grain becomes larger. The reason for this phenomenon can be explained as follows: in the case of high solution temperature, with the extension of holding time, the degree of large primary γ′ precipitates redissolved on the grain boundary increases, hence the γ matrix has enough supersaturation and nucleation density and a large amount of γ′ precipitates are reprecipitated during the cooling process. Under the rapid cooling rate (AC), there is not enough time and room for γ′ precipitates to grow, making the size of the γ′ precipitates become smaller. The morphology of γ′ precipitates is mainly dominated by isotropic interface energy because the lattice mismatch between γ/γ′ interfaces is small and can be ignored at this time. Therefore, in order to reduce the interface energy, the morphology of γ′ precipitates are mainly spherical, and the γ′ spherical and γ matrix are in a lattice coherent state [33].

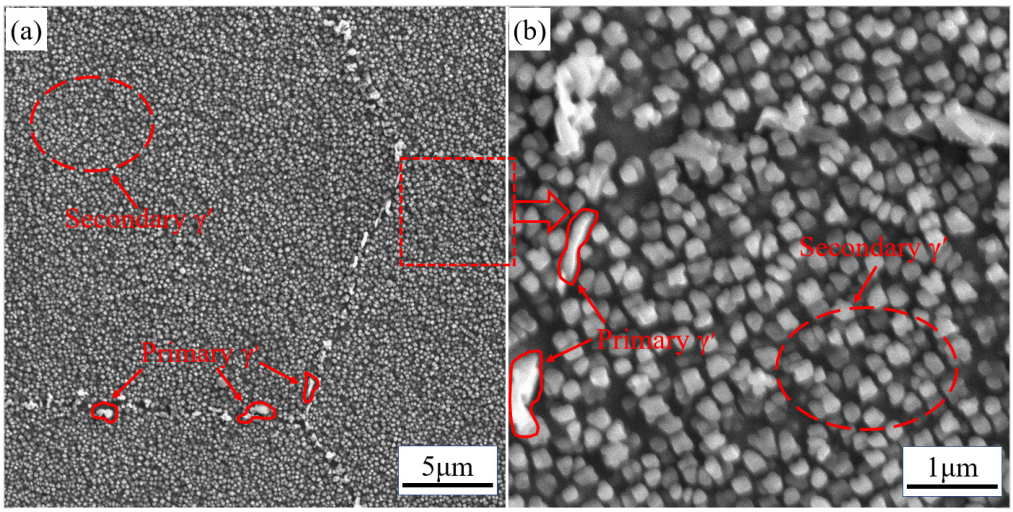


Figure 5. Morphology of γ′ precipitates after holding at 1100 °C for 1 h by AC: (**a**) low magnification, (**b**) high magnification and feature distribution of primary γ′ precipitates and secondary γ′ precipitates.

In summary, as the solution temperature increases from 1060 °C to 1100 °C, the average grain size decreases first and then increases compared with the incomplete dynamic recrystallization microstructure before heat treatment. At 1080 °C, due to the growth of recrystallized grains, a relatively uniform microstructure is formed between the recrystallized grains and the deformed grains, which makes the mean grain size minimum. The whole process is closely related to the dissolution degree of the initial γ′ precipitates. With the increase of the solution temperature, the large primary γ′ precipitates on the grain boundary dissolve more and more, and the hindering effect on the grain boundary migration becomes weaker. The recrystallized grains around the deformed grains continue to grow and gradually replace the deformed grains, making the grain boundaries straight. The supersaturation of the γ matrix and the nucleation density of the re-precipitated γ′ precipitates increase, resulting in the secondary γ′ precipitates with a small size and the tertiary γ′ precipitates with a smaller size being re-precipitated during AC. As the cooling mode

changes from AC to FC, the cooling rate and the nucleation density of the re-precipitated γ' precipitates decrease, which provides a large supersaturation for the γ matrix and a high diffusion rate for the γ' precipitates, making the γ' precipitates grow irregularly. At the same time, due to the larger chemical driving force along the <111> crystal direction than the <100> crystal direction, the re-precipitated γ' precipitates grow rapidly along the <111> crystal direction, causing the precipitates to split and form different morphologies. As the holding time of the solution treatment decreases from 10 h to 1 h, the degree of redissolution of the primary γ' precipitates decreases, the supersaturation of the γ matrix decreases, the nucleation density of the re-precipitated γ' precipitates decreases, and the size of the re-precipitated γ' precipitates increases compared with the holding time of 10 h under the same AC condition.

4. Conclusions

In this work, the incomplete dynamic recrystallization P/M nickel-based superalloy FGH4096 was treated by solution treatment at different temperatures, holding times, and cooling modes, and the effect on the size, morphology, and distribution of the grains and precipitates were analyzed. The following conclusions can be drawn:

1. With the increase of solution temperature, the recrystallization degree of the incomplete dynamic recrystallization structure gradually increases, and the average grain size first decreases and then increases when the temperature is increased 1060 °C to 1100 °C. With the increasing degree of redissolution of γ' precipitates on the grain boundary, the pinning effect to grain boundary becomes weaker, and the size of the secondary γ' precipitates within the grain becomes smaller and the volume fraction becomes larger.
2. The reprecipitated secondary γ' precipitates are mainly spherical under AC and have a bimodal distribution under FC. The morphology transforms from spherical to near-spherical, cuboids, octets, petaloid, and dendrites.
3. The γ' precipitates have a small size and large volume fraction due to high nucleation density and high cooling rate with the extension of holding time under a higher solution temperature (1100 °C).

Author Contributions: Conceptualization, Y.L.; methodology, Y.L.; software, M.W.; validation, Y.L.; investigation, M.W.; resources, Y.L.; data curation, M.W.; writing—original draft preparation, M.W.; writing—review and editing, M.W. and Y.L.; visualization, P.S.; supervision, G.Y. and W.S.; project administration, X.W.; funding acquisition, Y.L. All authors have read and agreed to the published version of the manuscript.

Funding: The present work received financial support of the National Natural Science Foundation of China (Grant No. 51805308), the Natural Science Foundation of Shaanxi Province (Grant No. 2019JQ-303), the China Postdoctoral Science Foundation (Grant No. 2018M631189).

Data Availability Statement: The data supporting the findings of this study are available from the corresponding author.

Conflicts of Interest: The authors declare no conflict of interest.

References

1. Williams, J.C.; Starke, E.A. Progress in structural materials for aerospace systems. *Acta Mater.* **2003**, *51*, 5775–5799. [CrossRef]
2. Pollock, T.M.; Tin, S. Nickel-Based Superalloys for Advanced Turbine Engines: Chemistry, Microstructure and Properties. *J. Propuls. Power* **2006**, *22*, 361–374. [CrossRef]
3. Hu, L.X.; Feng, X.Y. The research and development of powder metallurgy superalloy. *Powder Metall. Ind.* **2018**, *28*, 1–7. (In Chinese)
4. Zhang, X.; Chen, Y.; Hu, J. Recent advances in the development of aerospace materials. *Prog. Aerosp. Sci.* **2018**, *97*, 22–34. [CrossRef]
5. Pollock, T.M. Alloy design for aircraft engines. *Nat. Mater.* **2016**, *15*, 809–815. [CrossRef]
6. Guo, W.M.; Dong, J.X.; Wu, J.T.; Zhang, F.G.; Chen, G.S.; Chen, S.D. Microstructure and Properties of PM Superalloys FGH96. *J. Iron Steel Res.* **2005**, *17*, 59–63.
7. Ning, Y.; Yao, Z.; Fu, M.W.; Guo, H. Dynamic recrystallization of the hot isostatically pressed P/M superalloy FGH4096 in hot working process. *Mater. Sci. Eng. A* **2010**, *527*, 6968–6974. [CrossRef]

8. Li, F.; Fu, R.; Yin, F.; Feng, D.; Wang, H.; Du, G.; Feng, Y. Impact of γ′(Ni3(Al,Ti)) phase on dynamic recrystallization of a Ni-based disk superalloy during isothermal compression. *J. Alloys Compd.* **2017**, *693*, 1076–1082. [CrossRef]
9. Liu, X.T.; Ding, H.H.; Yang, C.; Liu, F.; Huang, L.; Jiang, L. Microstructure and mechanical properties of hot extruded FGH96 powder metallurgy superalloy. *Trans. Nonferrous Met. Soc. China* **2016**, *26*, 354–364.
10. Jia, C.L.; Ge, C.C.; Yan, Q.Z. Microstructure evolution and mechanical properties of disk superalloy under multiplex heat treatment. *Mater. Sci. Eng. A* **2016**, *659*, 287–294. [CrossRef]
11. Kim, I.S.; Choi, B.G.; Jung, J.E.; Do, J.; Seok, W.Y.; Lee, Y.H.; Jeong, I.Y. Effect of heat treatment on microstructural evolution and creep behaviors of a conventionally cast nickel-based superalloy. *Mater. Charact.* **2020**, *165*, 110378. [CrossRef]
12. Qiao, S.; Wang, Y.; Lv, L.; Huang, Z.; Tan, G. Normal and abnormal grain growth in a FGH96 superalloy during thermomechanical treatment. *J. Mater. Res. Technol.* **2021**, *15*, 7033–7049. [CrossRef]
13. Kumar, S.S.; Raghu, T.; Bhattacharjee, P.P.; Rao, G.A.; Borah, U. Evolution of microstructure and micro texture during hot deformation in an advanced P/M nickel base superalloy. *Mater. Charact.* **2018**, *146*, 217–236. [CrossRef]
14. Qiu, C.; Wu, X.; Mei, J.; Andrews, P.; Voice, W. Influence of heat treatment on microstructure and tensile behavior of a hot isostatically pressed nickel-based superalloy. *J. Alloys Compd.* **2013**, *578*, 454–464. [CrossRef]
15. Tian, T.; Hao, Z.; Li, X.; Jia, C.; Peng, S.; Zhu, Q.; Ge, C. Influence of aging treatment on microstructure and properties of a novel spray formed powder metallurgy superalloy FGH100L. *J. Alloys Compd.* **2020**, *830*, 154699. [CrossRef]
16. Ding, H.H.; He, G.A.; Xin, W.; Feng, L.; Huang, L.; Jiang, L. Effect of cooling rate on microstructure and tensile properties of powder metallurgy Ni-based superalloy. *Trans. Nonferrous Met. Soc. China* **2018**, *28*, 451–460. [CrossRef]
17. Huang, H.; Liu, G.; Wang, H.; Wang, Z.; Zhang, H.; Shao, Y.; Hu, B. Effect of cooling rate and resulting microstructure on tensile properties and deformation mechanisms of an advanced PM nickel-based superalloy. *J. Alloys Compd.* **2019**, *805*, 1254–1259. [CrossRef]
18. Han, Z.Y.; Zhang, P.X.; Song, J.M.; Wang, Q.X.; Liang, S.J.; Tang, B.; Lai, Y.J. Effect of Heat Treatment on Microstructure and Mechanical Properties of P/M Inconel 718 Superalloy. *Rare Met. Mater. Eng.* **2021**, *50*, 693–698. (In Chinese)
19. Zhang, L.; Li, D.; Qu, X.; Qin, M.; He, X.; Li, Z. Microstructure and tensile properties optimization of MIM418 superalloy by heat treatment. *J. Mater. Process. Technol.* **2016**, *227*, 71–79. [CrossRef]
20. Hao, Z.; Ge, C.; Li, X.; Tian, T.; Jia, C. Effect of Heat Treatment on Microstructure and Mechanical Properties of Nickel-Based Powder Metallurgy Superalloy Processed by Selective Laser Melting. *Acta Metall. Sin.* **2020**, *56*, 1133–1143. (In Chinese)
21. Tian, G.; Jia, C.; Liu, J.; Hu, B. Experimental and simulation on the grain growth of P/M nickel-base superalloy during the heat treatment process. *Mater. Des.* **2009**, *30*, 433–439. [CrossRef]
22. Liu, J.T.; Tao, Y.; Zhang, Y.W. Microstructure and mechanical property of FGH96 alloy dual property disk. *Trans. Mater. Heat Treat.* **2010**, *31*, 71–74.
23. Gabb, T.P.; Kantzos, P.T.; Telesman, J.; Gayda, J.; Sudbrack, C.K.; Palsa, B. Fatigue resistance of the grain size transition zone in a dual microstructure superalloy disk. *Int. J. Fatigue* **2011**, *33*, 414–426. [CrossRef]
24. Gao, J.; Luo, J.; Li, M.Q. Advance in manufacture technology and mechanism of aero-engine dual property disk. *J. Aeronaut. Mater.* **2012**, *32*, 37–43. (In Chinese)
25. Wu, H.; Zhuang, X.; Nie, Y.; Li, Y.; Jiang, L. Effect of heat treatment on mechanical property and microstructure of a powder metallurgy nickel-based superalloy. *Mater. Sci. Eng. A* **2019**, *754*, 29–37. [CrossRef]
26. Wan, Z.; Hu, L.; Sun, Y.; Wang, T.; Li, Z.; Zhang, Y. Effect of solution treatment on microstructure and tensile properties of a U720LI Ni-based superalloy. *Vacuum* **2018**, *156*, 248–255. [CrossRef]
27. Jiang, R.; Song, Y.D.; Reed, P.A. Fatigue crack growth mechanisms in powder metallurgy Ni-based superalloys—A review. *Int. J. Fatigue* **2020**, *141*, 105887. [CrossRef]
28. Mao, J.; Chang, K.M.; Yang, W.; Furrer, D.U.; Ray, K.; Vaze, S.P. Cooling precipitation and strengthening study in powder metallurgy superalloy Rene88DT. *Mater. Sci. Eng. A* **2002**, *332*, 318–329. [CrossRef]
29. Tian, G.F.; Jia, C.C.; Wen, Y.J.; Liu, G.Q.; Hu, B.F. Cooling γ′ precipitation behavior and strengthening in powder metallurgy superalloy FGH4096. *Rare Met.* **2008**, *27*, 410–417. [CrossRef]
30. Li, C.; Chen, L.L.; Qu, Z.H.; Lai, Y.J.; Liang, S.J. Measurement of complete dissolution temperature of γ′ phase in nickel-based P/M superalloy FGH4096. *Heat Treat. Met.* **2021**, *46*, 174–177. (In Chinese)
31. Lan, J.; Huang, H.; Mao, H.J.; Hua, L. Phase transformation and grain growth behaviors of superalloy IN718 during heat treatment. *Mater. Today Commun.* **2020**, *24*, 101347. [CrossRef]
32. Mitchell, R.J.; Preuss, M.; Tin, S.; Hardy, M.C. The influence of cooling rate from temperatures above the γ′ solvus on morphology, mismatch and hardness in advanced polycrystalline nickel-base superalloys. *Mater. Sci. Eng. A* **2008**, *473*, 158–165. [CrossRef]
33. Yu, H.; Wang, Z.; Zhang, B.; Ning, Y.; Fu, M.W. Re-precipitation mechanisms of the γ′ phase with sphere, near-sphere, cubic, octets and finally-dendrite in as-cast Ni-based superalloys. *J. Alloys Compd.* **2021**, *876*, 160104. [CrossRef]
34. Masoumi, F.; Shahriari, D.; Jahazi, M.; Cormier, J.; Devaux, A. Kinetics and Mechanisms of γ′ Reprecipitation in a Ni-based Superalloy. *Sci. Rep.* **2016**, *6*, 28650. [CrossRef]
35. Yoo, Y.S. Morphological instability of spherical γ′ precipitates in a nickel base superalloy. *Scr. Mater.* **2005**, *53*, 81–85. [CrossRef]
36. Fan, X.; Guo, Z.; Wang, X.; Yang, J.; Zou, J. Morphology evolution of γ′ precipitates in a powder metallurgy Ni-base superalloy. *Mater. Charact.* **2018**, *139*, 382–389. [CrossRef]

37. Breidi, A.; Allen, J.; Mottura, A. First-principles modeling of superlattice intrinsic stacking fault energies in Ni_3Al based alloys. *Acta Mater.* **2018**, *145*, 97–108. [CrossRef]
38. Qiu, C.L.; Andrews, P. On the formation of irregular-shaped gamma prime and serrated grain boundaries in a nickel-based superalloy during continuous cooling. *Mater. Charact.* **2013**, *76*, 28–34. [CrossRef]

Disclaimer/Publisher's Note: The statements, opinions and data contained in all publications are solely those of the individual author(s) and contributor(s) and not of MDPI and/or the editor(s). MDPI and/or the editor(s) disclaim responsibility for any injury to people or property resulting from any ideas, methods, instructions or products referred to in the content.